

SUPPORTING INFORMATION FOR

Impact of Dry Intrusion Events on Composition and Mixing State of Particles During Winter ACE-ENA Study

Jay M. Tomlin¹, Kevin A. Jankowski¹, Daniel P. Veghte^{3,4}, Swarup China⁴, Peiwen Wang⁵, Matthew Fraund⁶, Johannes Weis⁶, Guangjie Zheng^{7,8}, Yang Wang^{8,9}, Felipe Rivera-Adorno¹, Shira Raveh-Rubin¹⁰, Daniel A. Knopf⁵, Jian Wang^{7,8}, Mary K. Gilles⁶, Ryan C. Moffet¹¹, Alexander Laskin^{1,2*}

¹Department of Chemistry, ²Department of Earth Atmospheric and Planetary Sciences, Purdue University, West Lafayette, IN 47907, USA

³Center for Electron Microscopy and Analysis, Ohio State University, Columbus, OH 43212, USA

⁴Environmental Molecular Sciences Laboratory, Pacific Northwest National Laboratory, Richland, WA 99354, USA

⁵School of Marine and Atmospheric Sciences, Stony Brook University, Stony Brook, NY 11794, USA

⁶Chemical Sciences Division, Lawrence Berkeley National Laboratory, Berkeley, CA 94720, USA

⁷Center for Aerosol Science and Engineering, Department of Energy, Environmental and Chemical Engineering, Washington University in St. Louis, St. Louis, MO 63130, USA

⁸Environmental and Climate Science Department, Brookhaven National Laboratory, Upton, NY 11973, USA

⁹Department of Civil, Architectural and Environmental Engineering, Missouri University of Science and Technology, Rolla, MO 65409, USA

¹⁰Department of Earth and Planetary Sciences, Weizmann Institute of Science, Rehovot 76100, Israel

¹¹Sonoma Technology, Inc., Petaluma, CA 94954, USA

Correspondence to: Alexander Laskin (alaskin@purdue.edu)

TABLE OF CONTENTS

TABLE S1.....	3
FIGURE S1.....	4
FIGURE S2.....	5
FIGURE S3.....	6
FIGURE S4.....	7
FIGURE S5.....	8
FIGURE S6.....	9
FIGURE S7.....	10
FIGURE S8.....	11
FIGURE S9.....	12
FIGURE S10.....	13
TABLE S2.....	13
FIGURE S11.....	14

Summary of analyzed G1 aircraft samples

Sample date (YYYY-MM-DD)	TRAC hole no.	Sampling time (hh:mm:ss) (UTC)	Sampling altitude MSL (avg ± stdev.) (m)	Boundary layer height (m)	Dry intrusion event	Aerosol particle concentration (PCASP) (avg ± stdev.) (#/cm ³)	Wind speed (avg ± stdev.) (m/s)	Analysis	No. of particles analyzed
2018-01-19	33	14:14:55-14:24:56	288±351 (BL)	1000	No	76.3±47.9	6.1±1.7	CCSEM	842
2018-01-21	33	9:52:20-9:59:33	2673±4 (FT)	1600	No	15.8±4.0	11.9±2.6	CCSEM	1160
2018-01-21	36	10:13:29-10:20:32	153±4 (BL)	1600	No	42.3±6.7	11.7±0.6	CCSEM	1193
2018-01-21	46	11:23:54-11:30:57	1832±6 (FT)	1600	No	11.2±3.6	15.6±0.4	CCSEM	409
2018-01-21	48	11:38:00-11:45:03	40±6 (BL)	1600	No	33.9±7.6	12.7±0.5	CCSEM	1171
2018-01-21	53	12:13:15-12:20:18	1226±16 (BL)	1600	No	97.6±111.0	14.2±1.5	STXM	377
2018-01-21	58	12:48:27-12:55:30	1818±4 (FT)	1600	No	14.7±3.7	16.7±0.6	STXM	806
2018-01-24	42	13:31:46-13:38:49	227±145 (BL)	2100	Yes	32.7±6.0	7.0±0.6	CCSEM & STXM	1713 & 15
2018-01-24	49	14:21:07-14:28:10	1678±26 (BL)	2100	Yes	34.9±86.0	6.6±0.9	STXM	68
2018-01-24	51	14:35:14-14:42:17	2175±3 (FT)	2100	Yes	23.4±9.1	15.1±0.8	CCSEM & STXM	2991 & 28
2018-01-24	59	15:31:36-15:38:39	1029±5 (BL)	2100	Yes	28.4±27.3	6.0±0.7	STXM	283
2018-01-25	26	12:07:08-12:14:11	1366±10 (BL)	1650	Yes	55.2±26.7	2.9±1.2	CCSEM	2402
2018-01-25	28	12:21:13-12:28:16	1566±47 (BL)	1650	Yes	176.9±137.9	3.8±1.2	STXM	561
2018-01-25	42	13:59:51-14:06:53	1889±136 (FT)	1650	Yes	24.0±37.2	3.3±1.0	STXM	23
2018-01-25	44	14:13:56-14:20:59	879±560 (BL)	1650	Yes	61.2±26.6	3.3±1.1	STXM	166
2018-01-25	46	14:28:01-14:35:03	236±11 (BL)	1650	Yes	35.5±6.9	3.6±0.7	STXM	97
2018-01-26	39	11:49:55-11:56:58	1130±22 (BL)	1200	Yes	54±27.7	3.7±0.8	CCSEM	1216
2018-01-26	49	13:00:22-13:07:25	1408±394 (FT)	1200	Yes	63.9±91.4	4.4±0.5	STXM	467
2018-01-28	48	12:52:48-12:59:51	1866±2 (FT)	1700	No	18.1±5.1	8.9±0.5	STXM	398
2018-01-30	33	9:42:52-9:49:55	2485±160 (FT)	1650	No	23.8±9.6	6.8±0.9	CCSEM	3386
2018-01-30	44	11:00:25-11:07:28	1259±38 (BL)	1650	No	73.6±87.4	4.4±1.8	STXM	284
2018-01-30	64	13:21:21-13:28:24	1508±2 (BL)	1650	No	10.5±3.2	4.6±0.4	CCSEM & STXM	955 & 268
2018-02-01	47	12:11:29-12:18:32	787±137 (BL)	850	No	61.3±23.1	6.1±1.6	CCSEM	967
2018-02-01	58	13:29:02-13:36:04	43±8 (BL)	850	No	86.4±22.3	3.8±1.1	STXM	76
2018-02-08	47	14:53:14-15:00:16	157±10 (BL)	2150	No	73.8±10.0	9.3±0.8	CCSEM	949
2018-02-08	51	15:21:23-15:28:26	1479±3 (BL)	2150	No	31.2±6.5	8.1±0.7	CCSEM	912
2018-02-08	57	16:03:41-16:10:44	2347±23 (FT)	2150	No	17.8±6.8	11.6±0.4	CCSEM	1305
2018-02-11	66	14:16:06-14:23:09	1390±5 (BL)	1950	No	60.5±54.1	5.7±0.8	CCSEM	1053
2018-02-15	34	13:10:09-13:17:12	2450±7 (FT)	2150	Yes	13.3±3.8	10.0±0.9	CCSEM	1383
2018-02-15	42	14:06:33-14:13:36	1162±6 (BL)	2150	Yes	131.1±167.7	1.8±1.1	CCSEM	1022
2018-02-16	41	13:23:46-13:30:49	168±188 (BL)	2100	Yes	23.7±4.7	2.3±0.5	CCSEM	1524
2018-02-16	43	13:37:51-13:44:54	1057±3 (BL)	2100	Yes	26.0±9.6	4.4±0.9	CCSEM & STXM	1536 & 5
2018-02-16	48	14:13:05-14:20:08	2181±19 (FT)	2100	Yes	142.8±17.2	4.3±0.4	CCSEM & STXM	1331 & 10
2018-02-16	51	14:34:14-14:41:17	1888±4 (BL)	2100	Yes	200.5±522.8	1.6±0.9	STXM	34
2018-02-16	58	15:23:34-15:30:37	2193±5 (FT)	2100	Yes	131.1±26.8	3.2±0.6	CCSEM & STXM	1681 & 179
2018-02-16	66	16:19:58-16:24:01	1744±20 (BL)	2100	Yes	31.7±6.2	2.1±0.9	CCSEM	1362
2018-02-19	37	11:33:44-11:40:47	43±4 (BL)	1800	Yes	16.4±4.4	7.8±0.8	CCSEM & STXM	3429 & 11
2018-02-19	52	13:19:24-13:26:29	4045±14 (FT)	1800	Yes	37.2±8.2	4.1±1.9	CCSEM & STXM	1278 & 21
2018-02-19	54	13:33:32-13:40:35	4057±8 (FT)	1800	Yes	35.7±7.3	3.2±1.3	STXM	73
2018-02-19	58	14:01:44-14:08:47	4057±9 (FT)	1800	Yes	35.8±7.3	3.2±1.3	STXM	82

Table S1. Samples analyzed for the study by CCSEM and STXM/NEXAFS and parameter discussed (sample date, sampling time, average sampling altitude, average sampling altitude, boundary layer height, synoptic condition, average aerosol particle concentration, wind speed near sea level, and number of particles analyzed by each type of analysis).

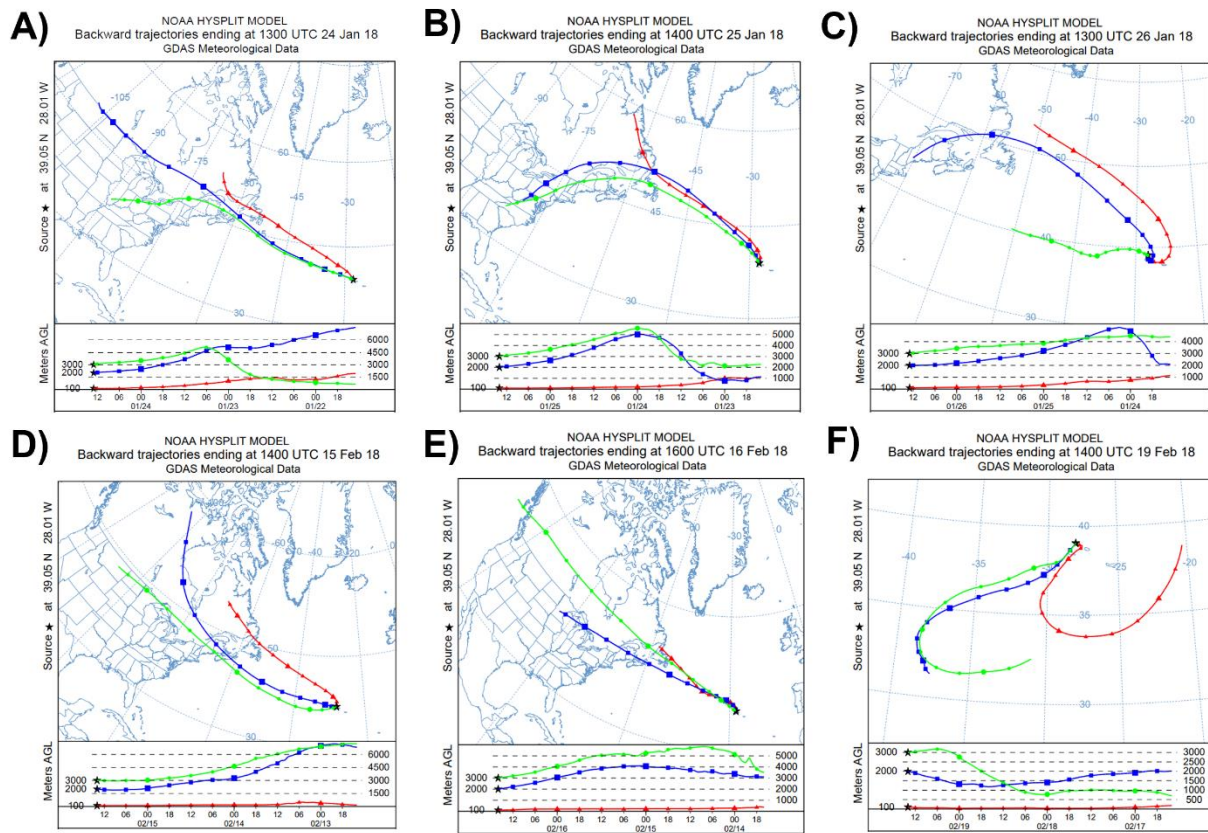


Figure S1. Hybrid Single-Particle Lagrangian Integrated Trajectory (HYSPLIT) (Stein et al., 2015; Rolph et al., 2017) back trajectories for dry intrusion periods utilizing global data assimilation system (GDAS1) achieved model data at three starting elevations 100 m (red), 2000 m (blue), 3000 m (green). A) 2018-01-24; B) 2018-01-25; C) 2018-01-26; D) 2018-02-15; E) 2018-02-16; F) 2018-02-19.

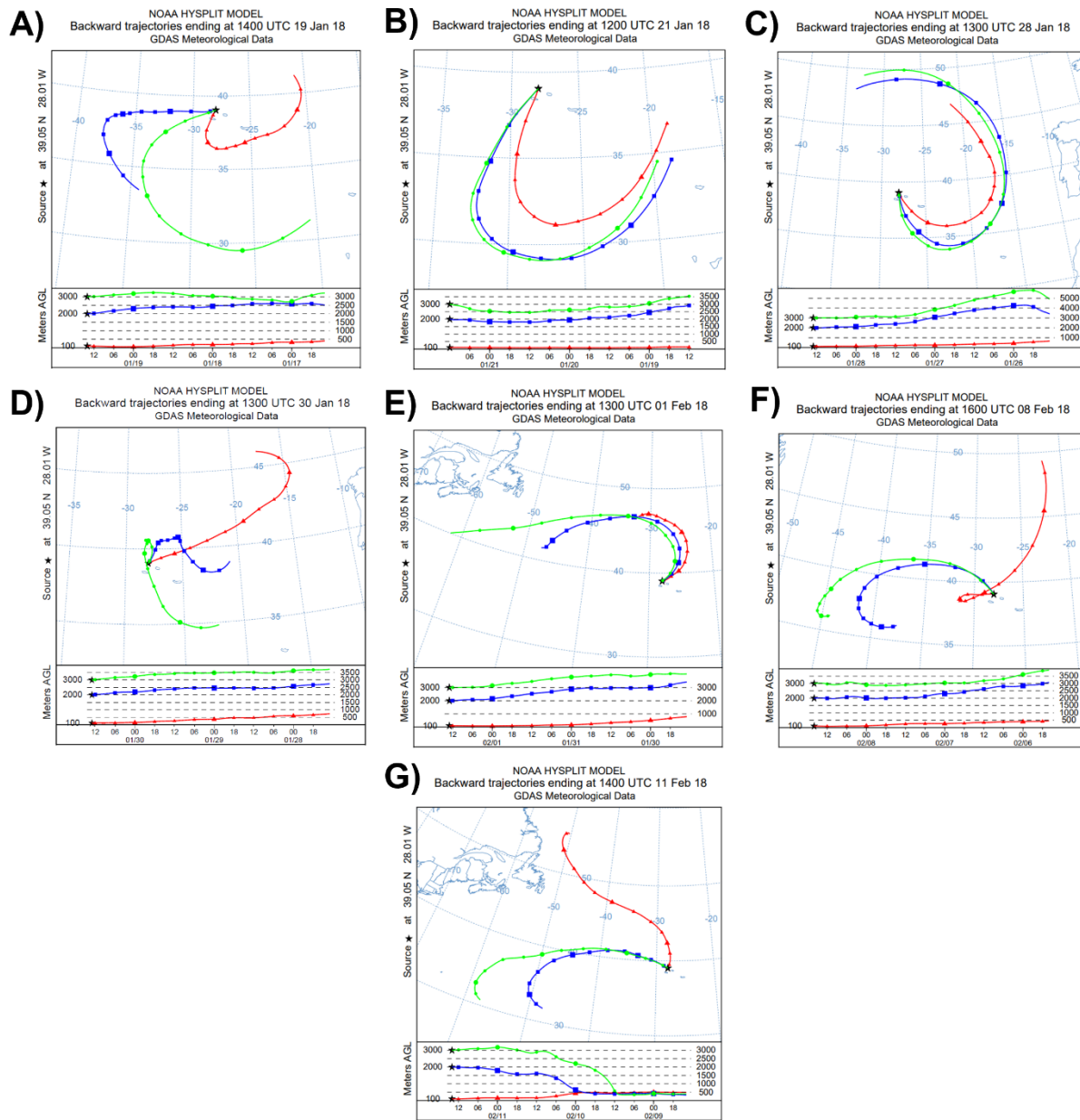


Figure S2. HYSPLIT back trajectories for each sampling day during non-dry intrusion periods utilizing GDAS1 achieved model data at three starting elevation 100 m (red), 2000 m (blue), 3000 m (green). A) 2018-01-19; B) 2018-01-21; C) 2018-01-28; D) 2018-01-30; E) 2018-02-01; F) 2018-02-08; G) 2018-02-11.

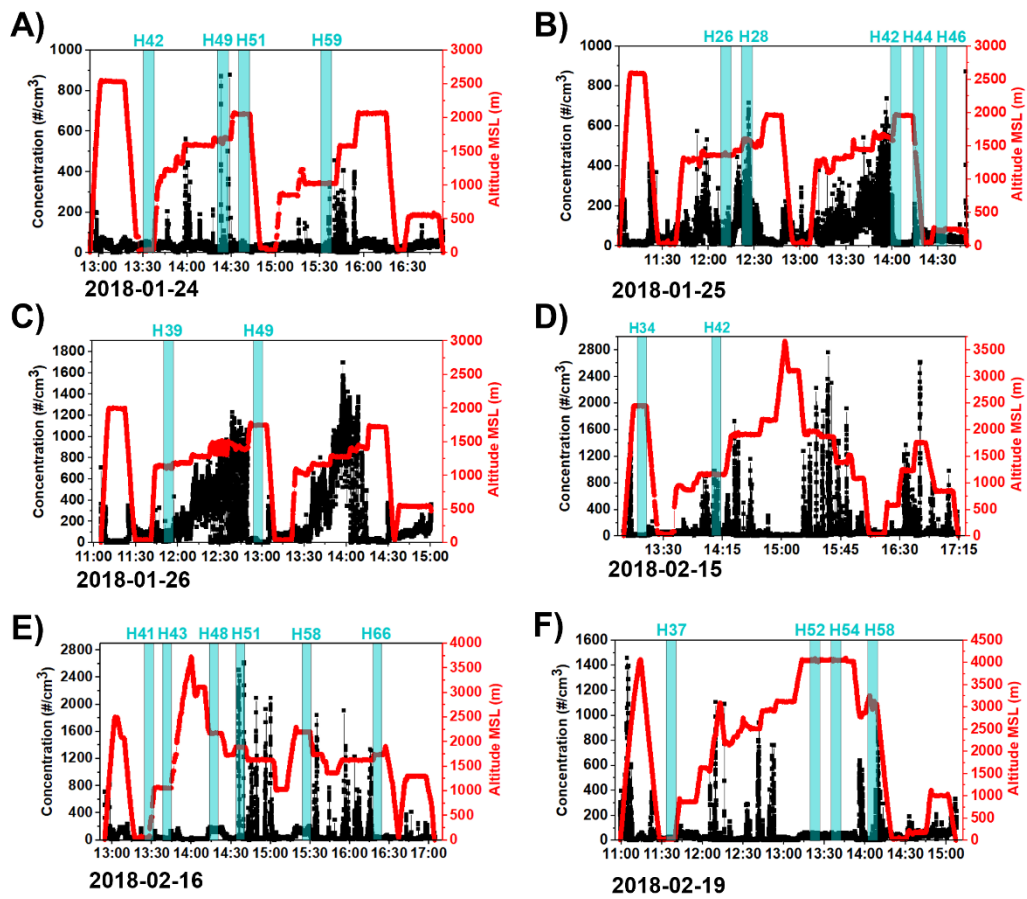


Figure S3. Flight summaries of altitude and particle concentration vs. time during dry intrusion periods: A) 2018-01-24; B) 2018-01-25; C) 2018-01-26; D) 2018-02-15; E) 2018-02-16; F) 2018-02-19. Blue shaded regions show time periods of particle sampling.

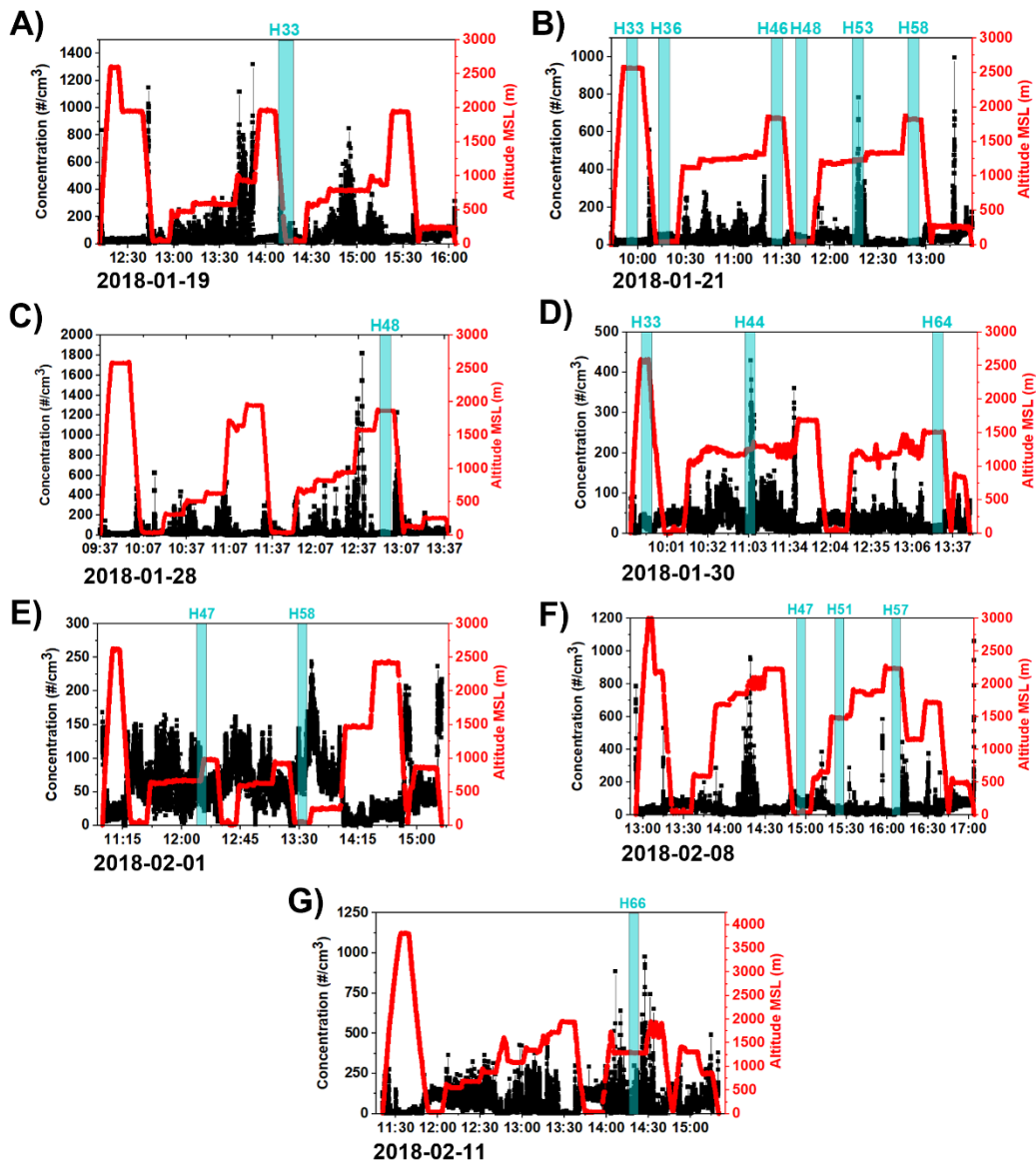


Figure S4. Flight summaries of altitude and particle concentration vs. time during non-dry intrusion periods: A) 2018-01-19; B) 2018-01-21; C) 2018-01-28; D) 2018-01-30; E) 2018-02-01; F) 2018-02-08; G) 2018-02-11. Blue shaded regions show time periods of particle sampling.

CCSEM-EDX particle classification schemes

All analyzed particles were combined before grouping into clusters using a *k*-means clustering algorithm (Hartigan and Wong, 1979) and utilizing the quantitative elemental contribution of 15 selected elements (e.g. C, N, O, Na, Mg, Al, Si, P, S, Cl, K, Ca, Mn, Fe, and Cu) acquired by the CCSEM/EDX analysis with Cu excluded in the analysis due to the material of the particle substrate. The square root of elemental contribution of individual particles were implemented in the *k*-means clustering to allow for the larger weighting of trace elements (Rebotier and Prather, 2007). The initial condition of the *k*-means algorithm is defined with eight initial centroids (i.e., cluster centers) for the entire data set. We then combined clusters with similar mean elemental contributions and narrowed the classification into four major clusters: (1) Mixed Sea Salt, (2) Aged Sea Salt, (3) Ammonium Nitrate/Sulfates, (4) Carbonaceous, as shown below.

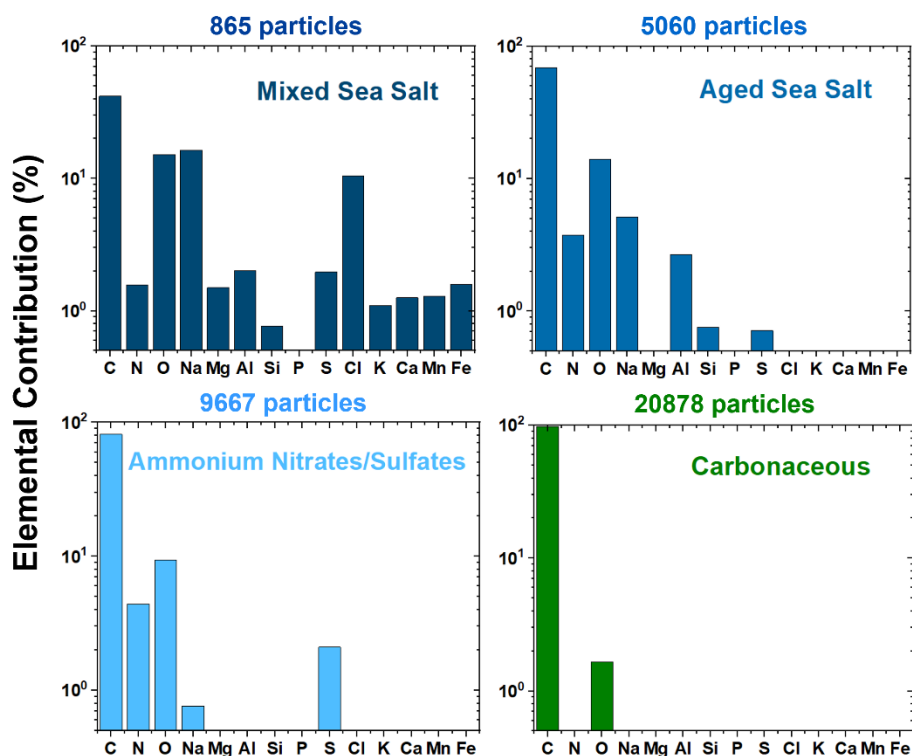


Figure S5. Mean elemental contribution (logarithmic scale) for each particle-type identified using clustering algorithm applied to all combined samples.

As a complementary analysis method, the rule-based classification scheme separates the particles into five different operator defined categories: “Sea Salt,” “Sea Salt/Sulfate,” “Sulfates/Organics,” “Carbonaceous,” and “Other.” Particle categories are first classified according to the Na content where if Na is greater than or equal the threshold value of 1%. These particles are further divided into separate classes of $[Na] > [S]$ classified as “Sea Salt”, whereas those of $[Na] < [S]$ classified as “Sea Salt/Sulfate.” Particles of $[Na] < 1\%$ are further classified as “Carbonaceous” if concentration of other elements excluding Na, Cl, S is $< 1\%$; Particles with $[C, N, O, S] \geq 0.5\%$ are classified as “Carbonaceous/Sulfate.” Particles not classified into either of the above four classes are placed into a single nonspecific category “Other”. The reported particle size used in this work is based on projected area equivalent diameter (AED, μm), which assumes a 2D projected image of the equivalent circle diameter of a particle silhouette as it is readily available from SEM data.

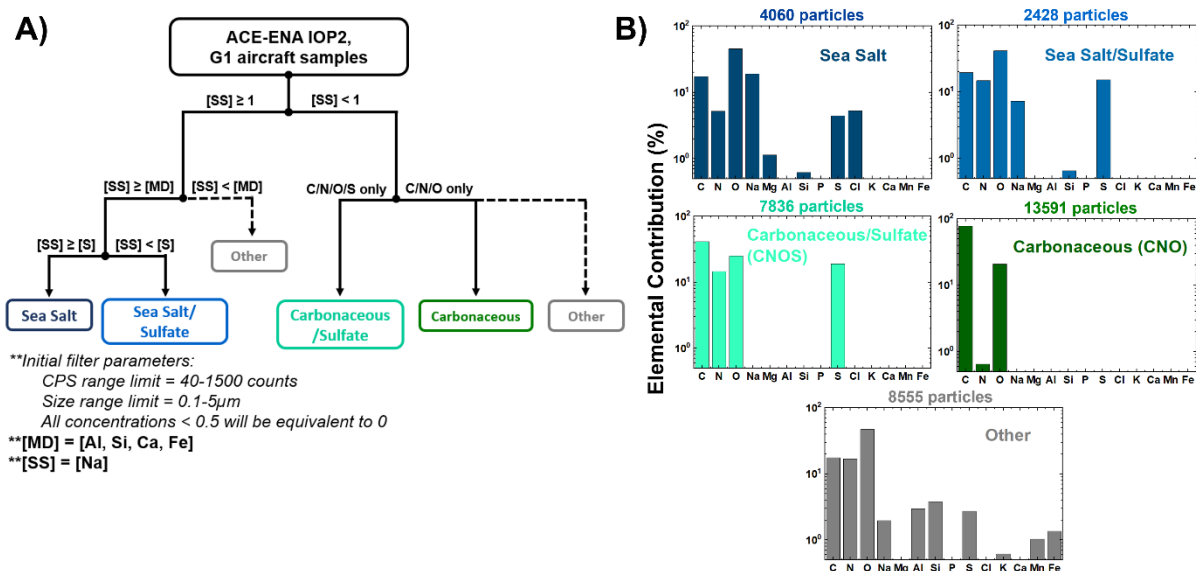


Figure S6. A) Classification scheme applied to particles from aircraft collected samples; B) Mean elemental contribution for each particle-type using rule-based method.

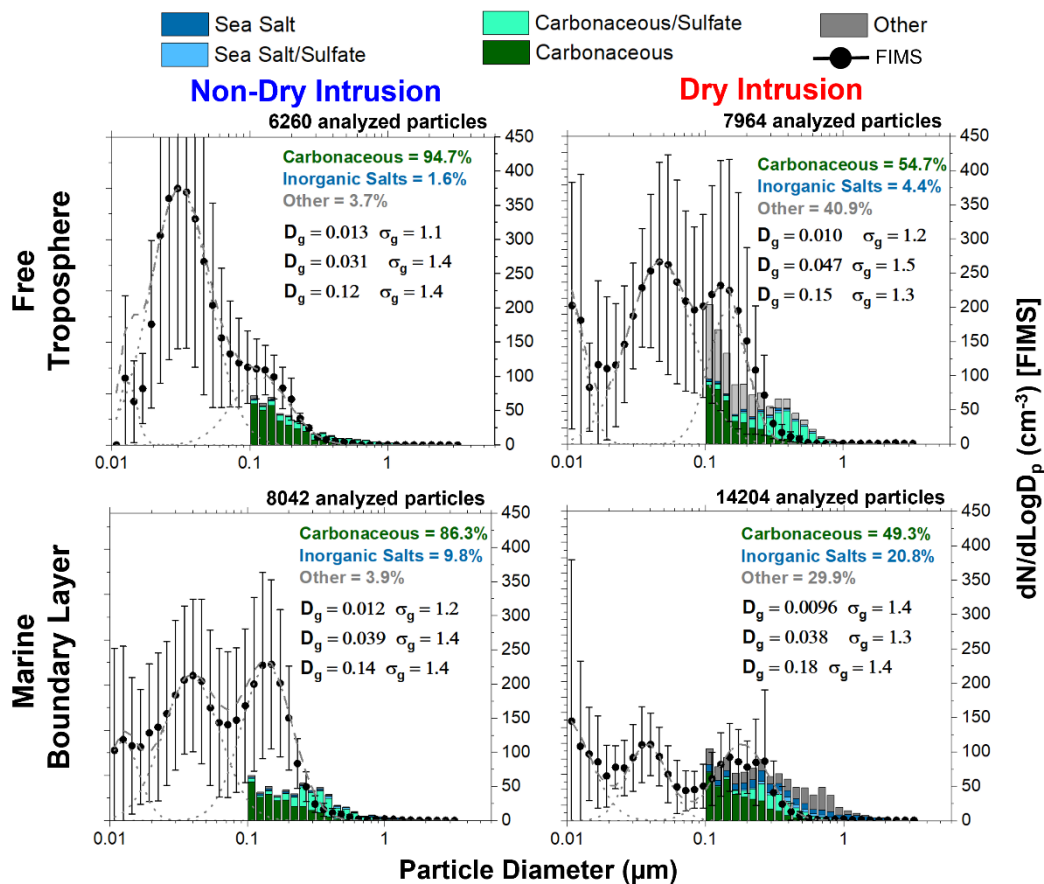


Figure S7. CCSEM size distribution rule-based particle classification scheme with average FIMS size distribution across different synoptic condition (non-dry intrusion vs. dry intrusion) and atmospheric layer (free troposphere vs. marine boundary layer) fitted with lognormal mode diameter (grey dashed lines). The CCSEM size distribution is superimposed and anchored at $0.25 \mu\text{m}$ as a visual comparison. The composition of the size-segregated particle-type population were broken down into “Carbonaceous” (i.e., Carbonaceous + Carbonaceous/Sulfate), “Inorganics” (i.e., Sea Salt + Sea Salt/Sulfate), and “Other”.

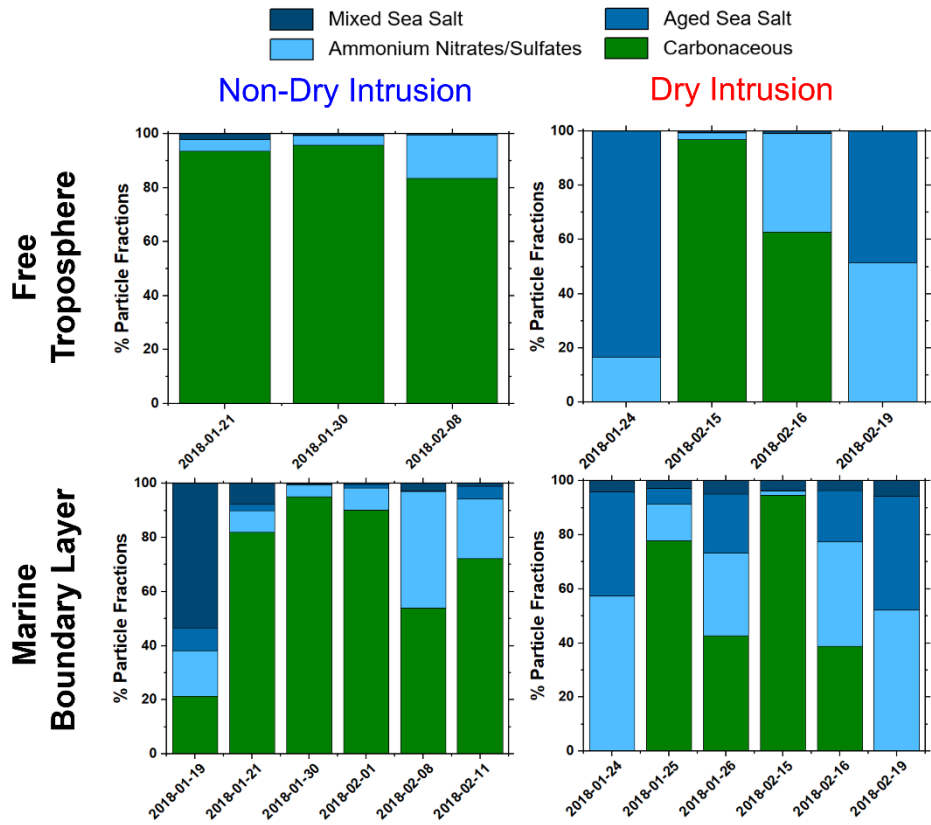


Figure S8. Particle-type fraction detected at different atmospheric layer (MBL vs. FT) and synoptic condition (non-DI vs. DI) for different research flights based on *k*-means clustering.

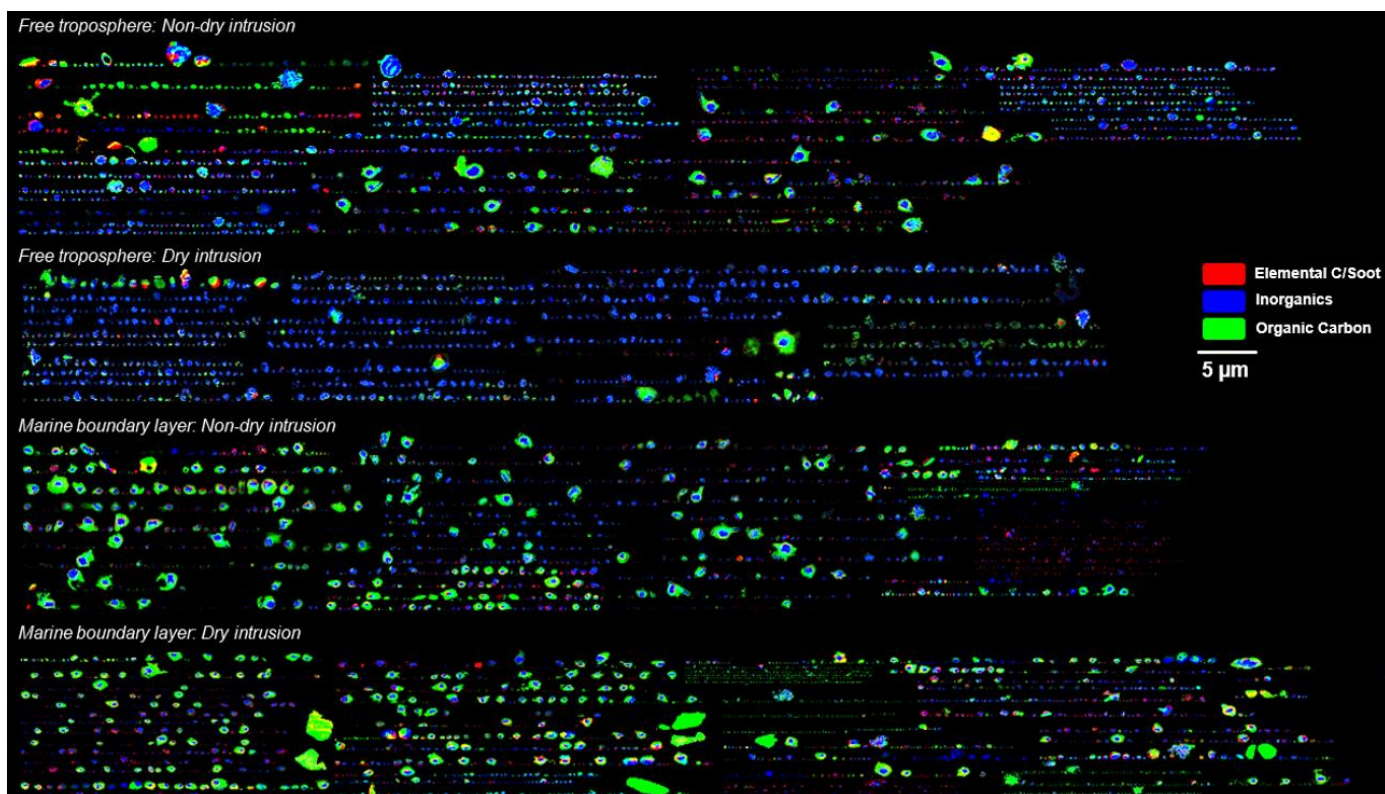


Figure S9. Collage of singular value decomposition map based on the STXM/NEXAFS imaging of particles in all analyzed samples collected at different atmospheric layer and synoptic conditions. Areas dominated by elemental carbon/soot components are shown in red, inorganic dominated regions are blue, and regions containing organic constituents are green. Note that components can overlap where each pixel can contain different combination of the individual components: EC + IN constituents as purple; OC + EC as yellow; OC + IN as cyan.

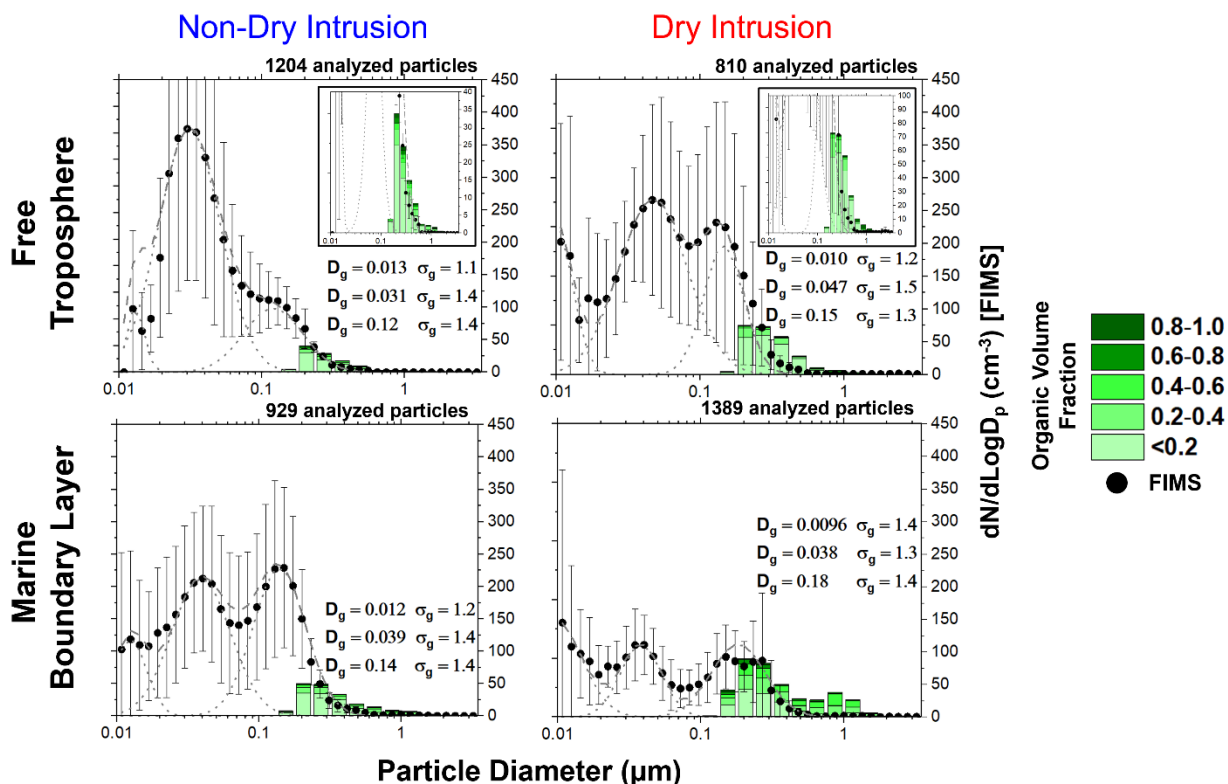


Figure S10. Size-resolved organic volume fraction ratio measured by STXM for individual particles superimposed with the particle size distribution measured by FIMS onboard the G-1 aircraft.

Component type	OVF Integrated Area		% Increase
	FT non-DI	FT DI	
NaCl-Sucrose	225.61	314.55	39.42
NaCl-Adipic acid	228.40	316.92	38.76
NaCl-Glucose	234.18	337.20	43.99
NaCl-Oxalic acid	262.04	379.73	44.91
(NH ₄) ₂ SO ₄ -Sucrose	151.64	158.16	4.30
(NH ₄) ₂ SO ₄ -Adipic acid	152.39	159.06	4.38
(NH ₄) ₂ SO ₄ -Glucose	155.99	163.37	4.73
(NH ₄) ₂ SO ₄ -Oxalic acid	168.80	188.17	11.48
Component type	OVF Integrated Area		% Increase
	MBL non-DI	MBL DI	
NaCl-Sucrose	356.48	921.19	158.41
NaCl-Adipic acid	358.14	915.13	155.52
NaCl-Glucose	364.93	959.31	162.88
NaCl-Oxalic acid	390.86	1138.52	191.28
(NH ₄) ₂ SO ₄ -Sucrose	246.79	426.69	72.89
(NH ₄) ₂ SO ₄ -Adipic acid	247.59	430.65	73.94
(NH ₄) ₂ SO ₄ -Glucose	254.13	465.22	83.07
(NH ₄) ₂ SO ₄ -Oxalic acid	276.98	571.60	106.37

Table 2. Calculated integrated area of STXM-derived organic volume fraction (OVF) for different inorganic-organic components. Relevant inorganic-organic components were chosen based on relevant particle-types in the region (i.e. marine environment) and previous literature used to calculate OVF (Fraund et al., 2019; Pham et al., 2017): Inorganic – NaCl, (NH₄)₂SO₄, Organic – sucrose, adipic acid, glucose, and oxalic acid. The integrated area was calculated by taking the sum of the percent contribution as a function of OVF as shown in Figure 6 applied for the different combinations of inorganic-organic components.

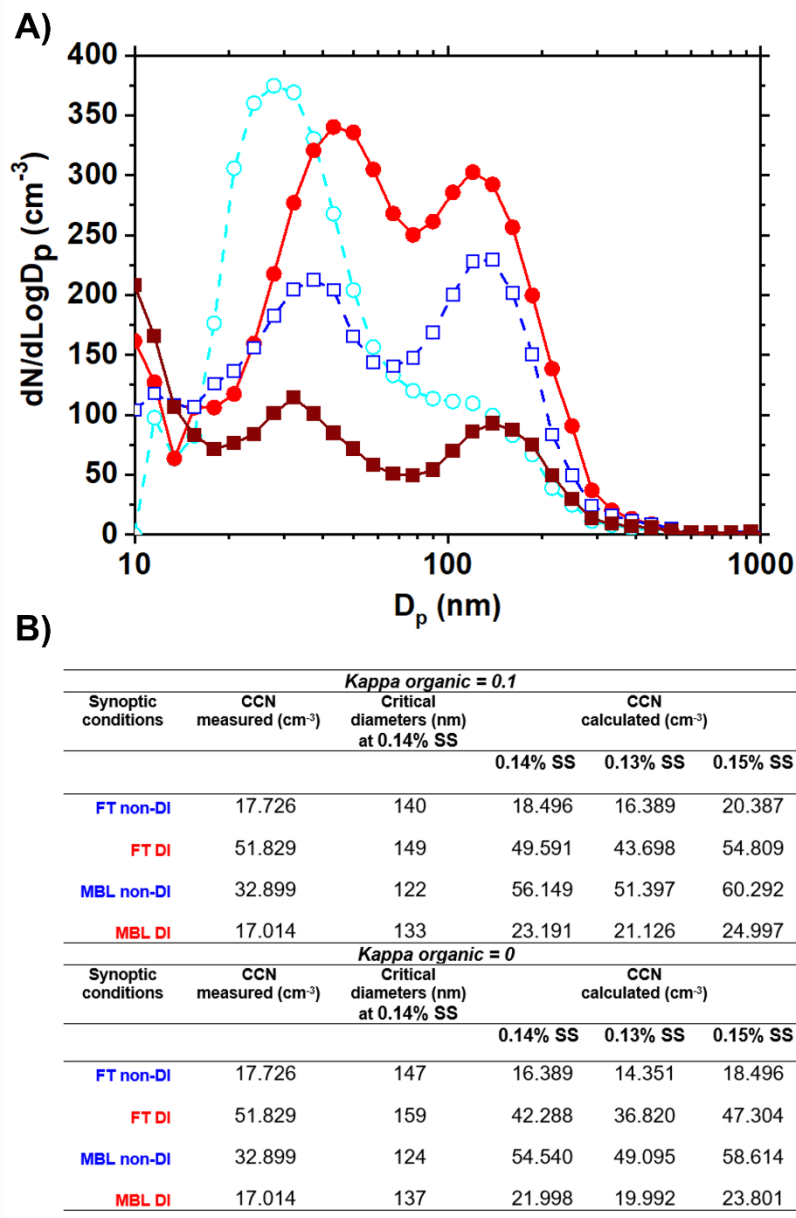


Figure S11. CCN activity of individual particles. A) Average FIMS particle size distribution for selected episodes during the ACE-ENA experiment. B) Comparison of measured and calculated CCN concentrations at different supersaturation (SS) values (0.13%, 0.14%, and 0.15% SS).

Reference

Fraund, M., Park, T., Yao, L., Bonanno, D., Pham, D. Q., and Moffet, R. C.: Quantitative capabilities of STXM to measure spatially resolved organic volume fractions of mixed organic/inorganic particles, *Atmospheric Meas. Tech.*, 12, 1619–1633, <https://doi.org/10.5194/amt-12-1619-2019>, 2019.

Hartigan, J. A. and Wong, M. A.: Algorithm AS 136: A K-Means Clustering Algorithm, *Appl. Stat.*, 28, 100–108, <https://doi.org/10.2307/2346830>, 1979.

Pham, D. Q., O'Brien, R., Fraund, M., Bonanno, D., Laskina, O., Beall, C., Moore, K. A., Forestieri, S., Wang, X., Lee, C., Sultana, C., Grassian, V., Cappa, C. D., Prather, K. A., and Moffet, R. C.: Biological Impacts on Carbon Speciation and Morphology of Sea Spray Aerosol, *ACS Earth Space Chem.*, 1, 551–561, <https://doi.org/10.1021/acsearthspacechem.7b00069>, 2017.

Rebotier, T. P. and Prather, K. A.: Aerosol time-of-flight mass spectrometry data analysis: A benchmark of clustering algorithms, *Anal. Chim. Acta*, 585, 38–54, <https://doi.org/10.1016/j.aca.2006.12.009>, 2007.

Rolph, G., Stein, A., and Stunder, B.: Real-time Environmental Applications and Display sYstem: READY, *Environ. Model. Softw.*, 95, 210–228, <https://doi.org/10.1016/j.envsoft.2017.06.025>, 2017.

Stein, A. F., Draxler, R. R., Rolph, G. D., Stunder, B. J. B., Cohen, M. D., and Ngan, F.: NOAA's HYSPLIT Atmospheric Transport and Dispersion Modeling System, *Bull. Am. Meteorol. Soc.*, 96, 2059–2077, <https://doi.org/10.1175/BAMS-D-14-00110.1>, 2015.